RSC Advances

PAPER

View Article Online
View Journal | View Issue

Cite this: *RSC Adv.*, 2025, **15**, 7209

The effect of the dual scale surface topography of a surface-modified titanium alloy on its bactericidal activity against *Pseudomonas aeruginosa*†

S. W. M. Amal Ishantha Senevirathne *[abd] and Prasad K. D. V. Yarlagadda [abcd]

The rapid advancement of antibacterial nanostructured surfaces indicates that they will soon be integrated into real-world applications. However, despite notable progress, a comprehensive understanding of the antibacterial properties of nanostructures remains elusive, posing a critical barrier to the translation of this *in vitro* technology into practical applications. Among the numerous antibacterial nanostructures developed, nanowire structures play an important role due to their enhanced efficacy against bacteria and viruses and their ease of fabrication. Antibacterial nanowire structures exhibit the dual capability of lysing bacteria upon surface adhesion and mitigating bacterial colonization. The interplay of surface energy significantly influences bacterial adhesion, and macro surface roughness appears to be a pivotal determining factor. Macro-scale surface roughness not only modulates surface energy but also results in micro-scale topographical features that impact the bactericidal efficacy of nanowire structures. The integration of nanofabrication techniques on surfaces with macro-scale roughness yields multi-hierarchical micro- and nanoscale features, thereby possibly amplifying the bactericidal effect. *Pseudomonas aeruginosa* is an opportunistic pathogen that can cause serious infections. Moreover, this species has a higher risk of developing antibiotic resistance, which makes treatments for infections extremely difficult. Nanowire structures have demonstrated higher efficacy against *P. aeruginosa* species, making it a good alternative for fighting *P. aeruginosa* infections. This study demonstrates that heightened surface roughness amplifies the bactericidal potency of nanowire structures against *P. aeruginosa bacterial* species. The bactericidal effect reaches its maximum when the average surface roughness value is close to the bacterial cell size. This is contrary to the conventional assumption that the substrate surface must be smooth for the nanostructures to work, as the nanowire structures exhibit robust bactericidal efficacy, even when fabricated on rough surfaces. Therefore, the applicability of bactericidal nanostructures is expanded beyond smooth substrates. Consequently, these nanostructures can be effectively deployed on rugged industrial surfaces, broadening their potential impact across a diverse array of sectors. The widespread adoption of this nanotechnology promises transformative benefits not only to the medical sector but also to various industries. Moreover, by curbing bacterial infections, nanostructured surfaces hold the potential to reduce mortality rates and yield more direct economic dividends through waste reduction and enhanced safety. Ultimately, the widespread implementation of antibacterial nanowire technology stands poised to improve societal well-being and quality of life.

Received 4th November 2024
Accepted 19th February 2025

DOI: 10.1039/d4ra07843h

rsc.li/rsc-advances

Introduction

The biomimicking of nanostructures has gained popularity over the last decade as it is potentially a winning strategy in the longtime battle against antimicrobial resistance. Bacteria are boundless, and they are both helpful and harmful to humans. While good bacteria benefit digestion,[1] the absorption of nutrients,[2] and the prevention of other harmful bacterial infections,[3] there are massive adverse effects caused by bacteria as well. Pathogenic infections are the most sensitive and destructive impact that bacteria have on humans. In 2019, there were 13.7 million deaths in the world due to infection related

[a]*Queensland University of Technology, Faculty of Engineering, School of Mechanical, Medical, and Process Engineering, Brisbane, QLD 4000, Australia. E-mail: s2.senevirathne@qut.edu.au; amal.ishan@gmail.com*

[b]*Queensland University of Technology, Centre for Biomedical Technologies, Brisbane, QLD 4000, Australia*

[c]*School of Engineering, University of Southern Queensland, Springfield Campus, Springfield Central, QLD 4300, Australia*

[d]*Australian Research Council Industrial Transformation Training Centre for Multiscale 3D Imaging, Modelling and Manufacturing, Australia*

† Electronic supplementary information (ESI) available. See DOI: https://doi.org/10.1039/d4ra07843h

complexities.[4] Nevertheless, the adverse effects of bacteria are not limited to the health sector and bacteria are known to create problems across varies industries. Microbial induced corrosion is one of the key adverse effects of bacteria which accelerates the corrosion of metals.[5–7] This corrosion affects steel reinforced concrete, pipelines, and many other metallic structures. Some examples of bacteria impacting industries adversely and causing exorbitant financial losses include, bacterial growth on marine vessel hulls that results in increased drag resistance,[8] reduced heat exchanger efficiency,[9] causing blockages in aviation fuel systems,[10] degrading aviation fuel,[11] and causing blockages in filtration mechanisms.[12] The food industry also suffers losses amounting to millions of dollars per year due to bacterial colonisation and related issues.[13,14] Making the situation worse is the ability of bacteria to evolve into strains that are resistant to antibiotics and antiseptics.[15] This makes infection treatments difficult or even impossible.[16] The Centers for Disease Control and Prevention in the United States of America estimates that 61 000 deaths per annum in the USA are due to antimicrobial resistant bacterial infections.[17] Moreover, $2.9 billion per year of economic losses in the USA have been caused by antimicrobial resistant bacteria.[18] In a global context, antimicrobial resistance has created enormous burdens on all nations alike.[19] According to the World Bank, if immediate remedies for antimicrobial resistance are not found, it may cost 3.8% of global annual gross domestic product (GDP) by 2050.[20] Therefore, the ability of bacteria to develop resistance to the current arsenal of antibiotics and antiseptics through the process of natural evolution, will soon render humankind defenceless against pathogenic microbes. As the current chemical antimicrobial agents are continuously overpowered by microbes through evolution, more potent chemical agents or alternative methods to kill bacteria are highly sort-after. The importance of antibacterial nanostructured materials is highlighted as an alternative method to kill bacteria without being susceptible to the threat of becoming obsolete.[21]

The discovery of the bactericidal properties of natural surfaces, such as cicada wings and dragonfly wings, has led to the development of new types of artificial bactericidal surfaces.[21] Currently two main theories are put forward to explain the mechanobactericidal action of nanostructured surfaces.[22,23] Nevertheless, both these theories are based on bacterial cell membrane failure due to mechanical stress exerted by sharp nanostructures. In addition, oxidative stress within the bacterial cells due to the sharp nanostructures is also presented as an alternative explanation to the mechanobactericidal effect.[24] Though conclusive evidence on bacterial death due to oxidative stress has been presented, it is largely disputed that oxidative stress is the sole or prominent cause of bacterial death on nanostructured surfaces. A careful review of the literature[25–29] indicates that the most logical explanation would be the combined effect of cell membrane failure under mechanical stress along with oxidative stress within the cell. Since its inception, the development of biomimicked antibacterial nanostructured surfaces has gained great momentum. Different types of nanofeatures have been tested for bactericidal effects, as well as many different substrate materials such as titanium, silicon, and polymers.[30–32] Moreover, with the aim of a successful translation of these nanostructures into end-user products, these nanostructured surfaces are tested under various conditions. For example, these nanostructures proved to be equally potent when they were fabricated on a 3-dimensional surface,[33] and the bactericidal efficacy is augmented when a fluid flow is present.[8,34] These studies have created much valuable knowledge on nanostructured surfaces, making them more appealing for use in industrial applications. However, there are many other aspects related to the nanostructured surfaces that should be understood for their seamless application in medical or industrial applications.

Among the many other parameters not examined, the initial surface roughness of the substrate plays an important role in both theoretical and practical aspects. As the surface roughness decreases, the surface area also decreases, which affects the surface energy. This in turn affects bacterial adhesion.[35,36] The surface roughness of a quartz substrate has shown a correlation between the surface roughness and bacterial adhesion on the surface.[37] Multiscale micro and nanostructures fabricated on aluminium have been reported to reduce bacterial adhesion and increase bactericidal efficacy.[38] Micro and nano scale multi-hierarchical structures fabricated on polypropylene have been reported to reduce bacterial adhesion by 82 to 86%.[39] A similar approach on polyethylene, with micron scale structures, has also reduced *E. coli* adhesion.[40] However, this multi-scale surface did not have any influence on the *S. aureus* species, indicating multiscale topographic surfaces display species specific behaviour. The species-specific performance of micro/nanostructures could be attributed to the cell membrane architecture, bacterial cell size and shape, and other factors such as the ability to form biofilms.[21,41–43] Although several reports on multiscale antibacterial topographies on polymeric surfaces could be found in the literature, very few studies have been reported on metallic surfaces. In one such report, dual scale sharp features at the micro and nano scales on a titanium substrate demonstrated an effect on both cell attachment and viability.[21,22] Nevertheless, the effect of micro scale surface topography on a surface with antibacterial nanostructures has not been previously studied. From a practical perspective, there are a range of surfaces on which nanostructures could be fabricated allowing for the potential applications of antibacterial nanostructures. Therefore, antipathogenic nanostructures should be able to be fabricated on surfaces with different surface finishes.

Nanostructures on titanium have demonstrated excellent bactericidal efficacy under various conditions. A variety of nanostructures such as nanopillars, nanocrystals, nanodarts, and nanowires fabricated on titanium have been reported. Among these, nanowires with very high efficacies of 98% against the *P. aeruginosa* species were recently reported.[44] This nanostructure has been studied extensively and is reported to have 60–70% efficacy against the *P. aeruginosa* species when tested under static conditions,[45,46] a similar efficacy when fabricated on a 3-dimensional curved substrate,[47] and a 98% efficacy under flow conditions.[34] Nanowires with tip diameters of ~50 nm and a height of ~300 nm have been identified as the

structures with the best bactericidal efficacy through extensive empirical examinations and computer simulations.[41,48,49]

Among the various types of nanostructures tested for antibacterial effects, it can clearly be seen that the demonstrated bactericidal effect is specific to the bacterial species. Nano pillar structures fabricated on titanium alloy tested against the *S. aureus* and *P. aeruginosa* species have shown selectively higher efficacy against the *P. aeruginosa* species.[50] This work studied 5 different nanopillar architectures with varying dimensions and reported higher efficacy against *P. aeruginosa* on all 5 surfaces. Another study reported that, while showing efficacies greater than 90% against the *P. aeruginosa*, *E. coli*, and *M. smegmatis* species, the nanopillar structures on titanium alloy showed a low efficacy against the *S. aureus* species.[51] In addition, numerous other studies reported that nanostructures have performed well against the *P. aeruginosa* bacteria compared to other species.[52–55] Moreover, the highest efficacies reported with nanostructures are against *P. aeruginosa*. Nanostructures with efficacies of 98%,[51] 98%,[53] 99%,[55] and 95% (ref. 34) against *P. aeruginosa* have been reported. Considering this trend, it can be concluded that nanostructures with antibacterial properties have the highest potential against *P. aeruginosa.*

In this study, the effect of the initial surface roughness of the substrate on the lysing bactericidal properties of titanium nanowire structured surfaces against the *P. aeruginosa* bacterial species is studied. The bacterial adhesion and bactericidal efficacy of nanostructured surfaces was studied by fabricating nanowires on substrates with varying surface roughness *via* a hydrothermal process.

Materials and methods

Substrate preparation

A Ti–6Al–4V 1 mm thick sheet was cut into 7 × 10 mm rectangular shaped pieces with one corner chamfered for easy identification of the side. A set of these pieces were polished using an electro-polishing process. Another 6 sets were sanded using 80, 120, 240, 400, 800, and 1500 grit sanding paper. All pieces were first sanded with 80 grit sanding paper, and a set of sanded pieces were separated and named as the 80 group. Then all pieces were sanded with 120 paper and another set was separated as the 120 group. This process was continued, and 6 groups of sanded pieces were obtained. Each group was labelled with the final sanding paper used on them, namely 80, 120, 240, 400, 800, and 1500.

Surface characterisation

Following the sanding process, the macro surface roughness of the 6 sanded groups and 1 polished group of substrates was measured using a Surtronic Profilometer. Measurements of the arithmetic average roughness (R_a) in μm taken across the surface lay with an accuracy of 0.01 μm and a cut-off length of 2.5 mm. Three measurements were taken for each sample with 3 samples taken from each group. One sample from each group was imaged using scanning electron microscopy (SEM) to observe the morphology of the surface before the hydrothermal reaction to fabricate nanowires on the surface. The arithmetic average surface roughness (R_a) and root mean square roughness (R_q) in nanometres (nm) along with the skewness were measured using atomic force microscopy (AFM). A Bruker AFM (Bruker Icon Dimension, Germany) was used with a Scanasyst tip in tapping mode. A scan size of 10 μm with 256 histogram bins and a 0.1 Hz scan rate was used. Then, 1st order flattening and 1st order plane fit with a 0.4 aspect ratio were used. Measurements were taken on 3 samples. The hydrophobicity of the samples, by means of the water contact angle, was tested both before and after the hydrothermal process using a Biolin ThetaFlex Drop Shape Analyzer. The water contact angle measurements were conducted using the Sessile drop measurement method. In brief, 5 μL of distilled water was used as the drop volume on the surface, and the average contact angle was measured after 5 seconds of drop settling time.

Nanofabrication

The 6 groups (80, 120, 240, 400, 800, 1500) of sanded surfaces and the one group of polished samples were subjected to a hydrothermal process, while one group of polished samples were separated as the control. The current protocol used for fabricating the nanowires on titanium requires that the surface is smoothed to a ~0.3 μm R_a surface roughness.[34] This same protocol was followed in all cases with the exception of the initial polishing process for the sanded surfaces. Seven groups were subjected to the hydrothermal process and were named as 0.25, 0.31, 0.40, 0.64, 0.87, 1.29, and 1.44 based on the mean surface roughness value for the respective group. The nanowire structure with a tip diameter of approximately 50 nm and a height of 300 nm fabricated using hydrothermal etching with sodium hydroxide was selected for the testing due to its excellent bactericidal and antiviral effect. The bactericidal effect of various nanowire heights and tip diameters has been studied previously. Therefore, the current study was planned to investigate the effects of the micro scale topography on bacterial adhesion and viability. All samples were sonicated at room temperature for 10 minutes in acetone, followed by washing with 80% ethanol thrice and with MilliQ water (Ultrapure Water Systems, Sartorius) thrice, before drying with $N_{2(g)}$. The samples were held in polytetrafluoroethylene (PTFE) holders and put inside 100 mL PTFE reactor vessels with 60 mL of 1 M $NaOH_{(aq)}$. The holder is designed to keep the samples inclined to prevent precipitation of gas bubbles during the hydrothermal reaction. The assembled hydrothermal pressure vessel was loaded into an oven at 180 °C and held for 2 hours at constant temperature. After 2 hours, the vessel was left to cool down inside the oven until the temperature dropped to ~60 °C, and then was left to cool inside a fume hood for a further 18 hours. Upon cooling, the substrates were retrieved from the pressure vessel and washed thrice with MilliQ water before drying with $N_{2(g)}$. Then, the samples were placed in crucibles and annealed inside a furnace at 300 °C for 1 hour at a heating rate of 10 °C min^{-1}. The substrates were left to cooldown overnight for approximately 18 hours. Next, the substrates were immersed in 0.6 M HCl acid for 30 minutes. Then the substrates were washed

thrice using MilliQ water before drying with $N_{2(g)}$. Following the ion exchange step, the samples were calcinated by heating to 600 °C at a rate of 10 °C min^{-1} and held under constant temperature for 2 hours. Once the samples were cooled to room temperature, they were retrieved and checked using SEM for the quality of nanowire fabrication.

Preparation of culture and buffer media

Nutrient broth was made using 26 g of nutrient broth powder (Oxoid, USA) dissolved in 1 L of MilliQ water to make 1 L of nutrient broth. The prepared nutrient broth was sterilised by autoclaving at 121 °C for 20 minutes (Tomy autoclave, SX700). Phosphate-buffered Saline (PBS) was prepared by dissolving a 1× PBS tablet (Oxoid, USA) in 500 mL of MilliQ water. PBS was also sterilised by autoclaving at 121 °C for 20 minutes.

Antibacterial testing

A *P. aeruginosa* (ATCC 27853) cell suspension was prepared by incubating a colony of bacteria streaked on 5 mL of nutrient broth for 16 hours in a shaking incubator at a 200 rpm speed at 37 °C (Beckman Coulter, Allegra X-15R centrifuge). Following the incubation, the colonies were retrieved from the nutrient broth suspension by centrifuging at 5250 rpm for 5 minutes at 37 °C, and the pellet was resuspended in sterile PBS. The bacterial concentration was quantified using a BioPhotometer by means of suspension turbidity measured on the OD_{600} scale following a protocol specified in the literature.[56] The suspension was diluted with sterile PBS until a turbidity level of 0.1 was reached. This approximates to 1×10^8 CFU mL^{-1} of cell concentration.[57] Then, 1 mL of turbidity-adjusted bacterial suspension was added to a microwell with the substrate inside in a 48-well plate. The cells were left to incubate on the titanium surface for 1 hour. Immediately following the incubation, the substrate was retrieved from the microwell allowing the wetting liquid to drain and transferred to a new microwell and the supernatant fluid was allowed to drain on the surface. Epi-fluorescence stain was prepared with a Live/Dead Baclight kit (Invitrogen detection technologies, L7012). Subsequently, 5 μL of Syto9 and Propidium Iodide was pipetted into 1 mL of sterilised deionised water in the dark to prepare the dye mixture for staining. Then, 3 μL of dye mixture was pipetted onto the substrate and was kept within a microwell in the dark. After 15 minutes of incubation, the substrates were transferred to glass-bottomed microslides for epifluorescence microscopy. A Nikon Eclipse Ti–S inverted fluorescence microscope using a 40× objective lens with a 0.6 numerical aperture with FITC and CY3 filters was used to image the live and dead bacterial cells, respectively. Each sample was imaged in 10 scattered locations with each location imaged with FITC and CY3 filters with a 100 ms exposure time. The filter change time was kept very short to minimise the time difference between the live and dead images. Images were taken scattered on the substrate to obtain a better representation of the substrate as well as to minimise the effect of dye bleaching due to the incident light beam caused by the prolonged time. Each image captured a 206.40×165.12 μm^2 area of the substrate with a resolution of 1280×1024 pixels. Cell quantification was done following a protocol in the literature.[58,59] Imaged files were saved by the microscope software package in its native file format of *.nd2* enabling accurate post-processing of the files. Fiji – ImageJ (Ver 1.53t) was used to process the images. First the colour balance of each image was adjusted to improve the contrast, followed by thresholding to binarize the image. The number of illuminated pixels in the binarized image was read using the BioFilmAnalyser software.[60] This pixel count of the binarized image was taken as being equivalent to the bacterial surface coverage as specified in the literature.[58] The number of live cells were counted by means of the pixels from the binarized image taken with the FITC filter, while the dead cell count was taken from the binarized image taken with the CY3 filter at the same location. The total cell count was taken as the sum of the live and dead cell counts at each location (image). Bactericidal efficacy was taken as the percentage of dead cells out of the total cell count. Two controls were used to verify the function of the stain. A 3 μL aliquot of bacterial suspension was used to verify the SYTO9 and FITC functionality, while 3 μL of another suspension treated with 70% v/v ethanol was used as the control for PI and CY3. Two controls were both stained with the dye mixture and labelled as Live-cell control and Dead-cell control, respectively. Each experiment was repeated three times.

Statistical analysis

ANOVA was used to analyse the variation between the different surface roughness groups in bacterial adhesion onto the surface and the bactericidal effect demonstrated by the surface. A confidence interval of 95% was used. Cell adhesion onto the surface (*i.e.* total cell count), bactericidal efficacy, live cell count, and dead count were compared using ANOVA. Bactericidal efficacy was defined as the percentage of dead cells on the surface out of the total number cells (both live and dead) found on the surface. First, all nanostructured groups were compared against the same response variable of the control surface, which is a polished surface without nanostructures on it (*i.e.* without hydrothermal treatment). Next all nanostructured groups were compared against each other. GraphPad Prism (version 10) software was used for all statistical analyses. Error bars shown in the graphs are the standard error of the mean calculated using eqn (1), where, n is the sample size and $\bar{x}$ is the mean of variable x.

$$\text{Std error of mean} = \frac{\sqrt{\dfrac{\sum_{i=1}^{n}(x_i - \bar{x})^2}{n-1}}}{\sqrt{n}} \quad (1)$$

Correlation analysis was used to test if the surface roughness does have a correlation with bacterial cell adhesion onto the surface and bactericidal efficacy demonstrated by the nanostructured surface. The Pearson correlation coefficient (r) was calculated using eqn (2) with the GraphPad Prism software, where x and y are the individual data points of the two variables, $\bar{x}$ is the mean of variable x, $\bar{y}$ is the mean of variable y, and n is

the sample size. A null hypothesis of "no correlation exists between the surface roughness and the other variables (bacterial adhesion, bactericidal efficacy of the nanostructured surface)" was created.

$$r_{x,y} = \frac{\sum_{i=1}^{n}(x_i - \overline{x})(y_i - \overline{y})}{\sqrt{\sum_{i=1}^{n}(x_i - \overline{x})^2}.\sqrt{\sum_{i=1}^{n}(y_i - \overline{y})^2}} \quad (2)$$

Regression analysis was used to estimate the effect of the surface roughness on the two variables (bacterial adhesion and bactericidal efficacy of the surface). The coefficient of determination (R^2) was used to represent the goodness of fit and was calculated using eqn (3) with the GraphPad Prism software, where a is the observed data point, f is the predicted value with the model, $\bar{a}$ is the mean, and n is the sample size.

$$R^2 = 1 - \frac{\sum_{i=1}^{n}(a_i - f_i)^2}{\sum_{i=1}^{n}(a_i - \bar{a})^2} \quad (3)$$

SEM imaging

All samples with bacteria were fixed with 2.5% glutaraldehyde in PBS. Following the fixation, samples were washed with PBS thrice to remove the glutaraldehyde and sequentially dehydrated with increasing concentrations of ethanol. Starting with 20% ethanol, the samples were drenched in ethanol and processed in a PELCO BioWave Pro microwave processer for 40 seconds. The same process was repeated with 30%, 40%, 50%, 60%, 70%, 80%, 90%, and 100% ethanol, except that with the 90% and 100% ethanol, each step was done two times. Following ethanol dehydration, the samples were dried with hexamethyldisilazane (HDMS). The samples soaked in HDMS were processed twice in the BioWave for 1 minute, and after the second cycle, the samples were left to air dry inside a fume hood overnight. After the dehydration process, the samples were coated with a 5 nm layer of gold. The samples without bacteria were also coated with a 5 nm layer of gold for better SEM images.

Results

Surface roughness, surface morphology, and hydrophilicity of the titanium substrates

The surface roughness measurements after the surface finishing processes and the water contact angle measurements before and after the hydrothermal treatment are shown in Fig. 1A and B, respectively. Progressive sanding resulted in reduction of the surface roughness, and the finest surface finish resulted from polishing, which yielded a 0.25 ± 0.05 μm R_a surface roughness, whilst 80 grit sanding paper caused the highest surface roughness of 1.44 ± 0.19 μm R_a. A water contact angle of up to 90° is hydrophilic and above 90° is hydrophobic.[61] The 0.25 μm R_a rough surface and 1.44 μm R_a rough surface were hydrophilic before the hydrothermal treatment according to the aforementioned criteria, and the rest of the surfaces were hydrophobic. However, the hydrothermal treatment made all surfaces hydrophilic, with the exception of the 1.29 μm R_a surface which became super-hydrophilic (water contact angle < 10°).

The R_a values obtained from the AFM analysis are shown in Fig. 1C and indicated that no statistically significant difference in nanoscale surface roughness between the flat–flat or nano–nano surface groups, except in one instance of the flat surfaces and two instances of the nano surfaces. The nanoscale R_a of the 0.25 μm R_a group was significantly different from the 1.44 μm R_a group for both the flat and nano surfaces, but the 1.29 nano surface also had a difference of 0.25 μm R_a with the nano surface group (data shown in the ESI†). Nevertheless, the surfaces with nanowires had higher roughness (R_a) than the same surface without the nanowires. As shown in Fig. 1C, a similar trend was observed for the root mean square roughness (R_q) as well. For the surfaces both with and without nanowires, the 1.29 and 1.44 μm R_a groups were different from the 0.25 μm R_a group. Skewness measurements indicated that most of the nanowire structured surfaces had prominent peaks rather than a flat surface with corresponding micro scale roughness, as shown in Fig. 1D. The 3D images obtained by AFM are shown in Fig. 2. Sharp nanowires as well as the microscale texture underlying on the surface can be clearly observed in the AFM images. Microscale deep trenches can be seen in the AFM images confirming the observations in the SEM images shown in Fig. 4. The sharpness of the nanowires is visualised better in the AFM images than in the SEM images.

Bacterial cell morphology on the nanowire structured surfaces

Fig. 3 shows the scanning electron microscopy (SEM) images of the (A) dead *P. aeruginosa* cells on the nanowires, (B) the live cells on the nanowires, (C) the dead cells on the smooth (control) surface, and (D) the live cells on the smooth surface. Live cells on both surfaces have similar morphologies that resembles an inflated elongated balloon. However, there is a drastic contrast between the dead cells on the nanowires and the smooth surface. The dead cells on the nanowires are flatten, while the dead cells on the smooth surface looks partially deflated.

Fig. 4 shows the SEM images of the substrates, after surface finishing processes (sanding or polishing), after the hydrothermal process to fabricate the nanowire structures, and after incubation with *P. aeruginosa* bacteria for 1 hour under static conditions. The polished surface had no noticeable surface lay in the SEM images. When the hydrothermal treatment was done, the nanowires formed an even top surface that resembles the initial surface. However, the surfaces roughened with sanding, showed unidirectional surface scratches in the SEM images. These unidirectional markings became deep and wide as the surface roughness increased. Once the nanowires were fabricated on the surface, the top surface can be seen to be wavy, and the waviness increased with the surface roughness. Surfaces with high roughness (0.87, 1.29, and 1.44 μm R_a) had scratches with tips and gorges. The topography of these surfaces can be categorised into three distinct regions based on the topography. Deep trenches with valleys at the bottom and peaks at the top are

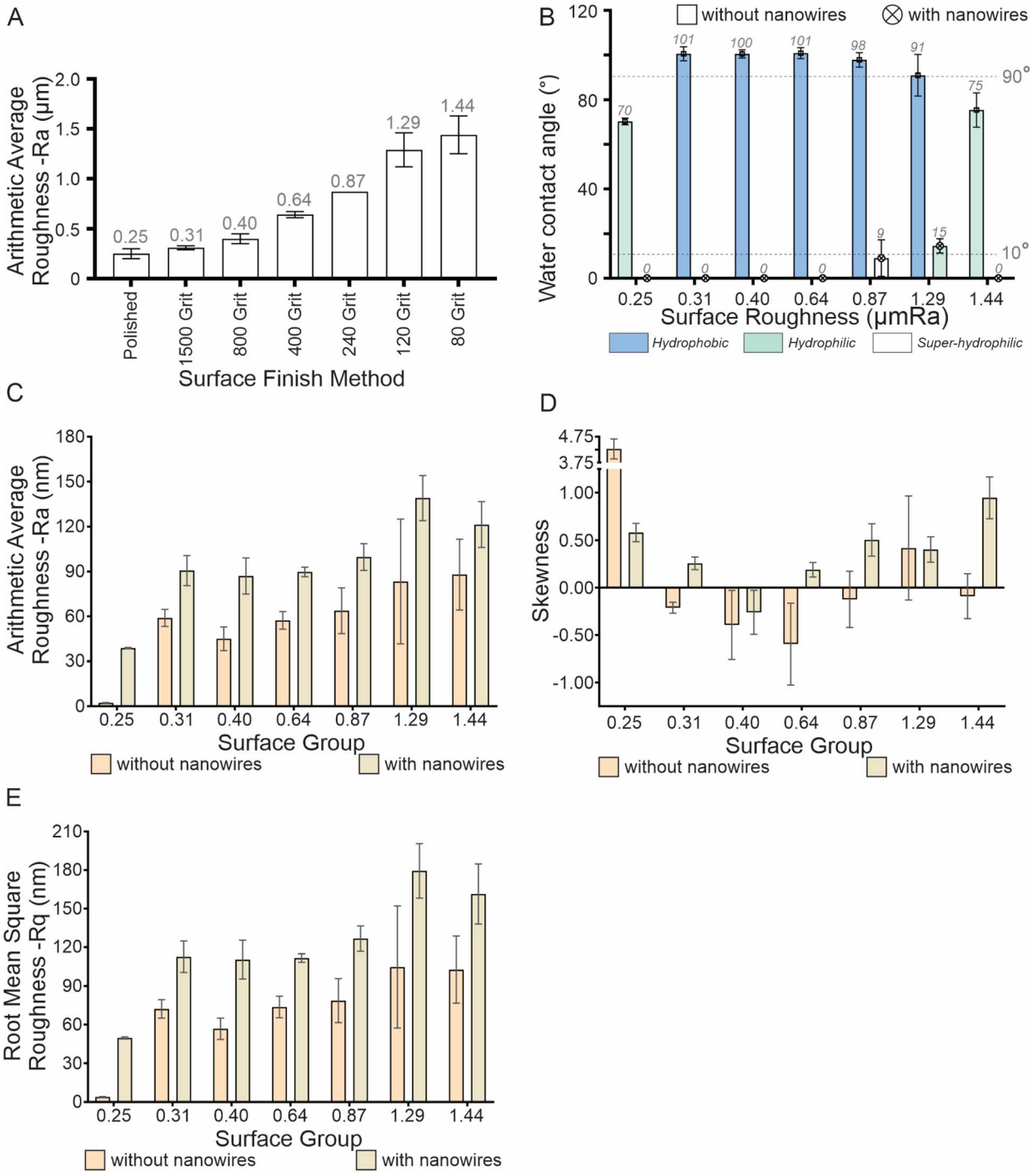

Fig. 1 (A) Surface roughness measurements given as the arithmetic average surface roughness (μm) of the titanium substrates finished with polishing and sanding with increasing grit number (= reducing grit size). (B) Water contact angle (WCA) of the substrates before and after fabricating nanowires using hydrothermal reaction process. Values shown are the average of 3 measurements. Data given in Table SI 1.† When WCA ≤ 90°, the surface is hydrophilic and when WCA < 10° it is considered to be super-hydrophilic. (C) Arithmetic average surface roughness R_a (nm) obtained using atomic force microscopy (AFM) (D) skewness of the surface, (E) root mean square roughness R_q (nm) obtained using AFM.

highly distinguishable. In addition to the peaks and valleys, plateau areas were also observed either at the bottom or the top. Interestingly, higher concentrations of bacteria can be seen in the valley areas of those surfaces. While the plateau areas had fewer cells than the valleys, the narrow peaks had very few cells on them. As the surface roughness decreases, the three regions (peaks, valleys, and plateaus) became less prominent. The 0.64 μm R_a surface had some deep trenches, but the peaks were not present. The 0.40, and 0.31 μm R_a surfaces, had shallow trenches on them with no distinguishable peaks.

Fig. 5 shows the fluorescence images of the 7 groups of substrates (B–H) with nanowire structures and the 1 group of

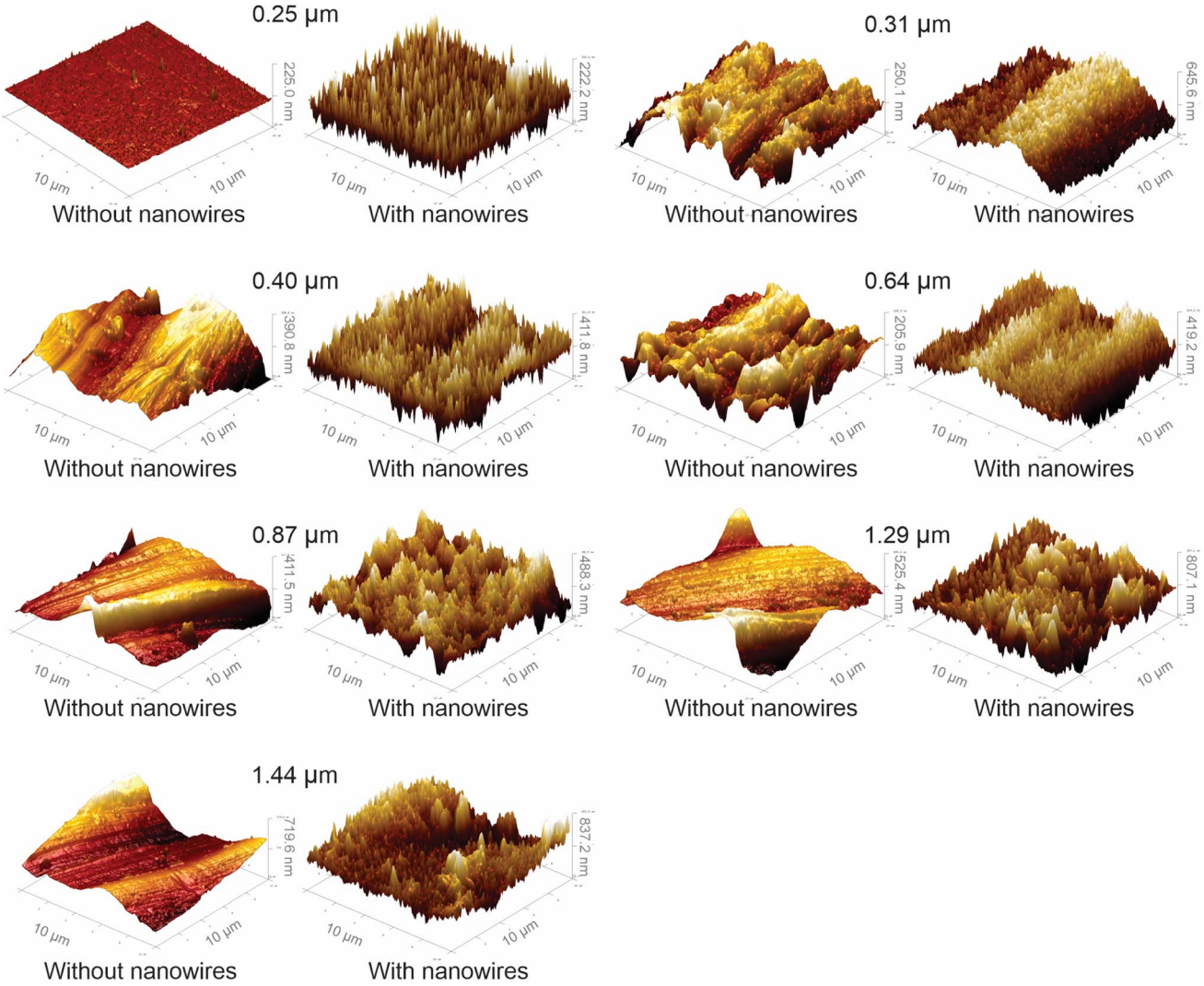

Fig. 2 Atomic force microscopy images of seven surface groups before and after hydrothermal treatment. Each scan was taken in a 10 µm × 10 µm area on the surface. Atomic force microscopy (AFM). Bruker AFM (Bruker Icon Dimension, Germany) was used with Scanasyst tip in tapping mode. A scan size of 10 µm with 256 histogram bins and 0.1 Hz scan rate was used. 1st order flattening, and 1st order plane fit with 0.4 aspect ratio was used.

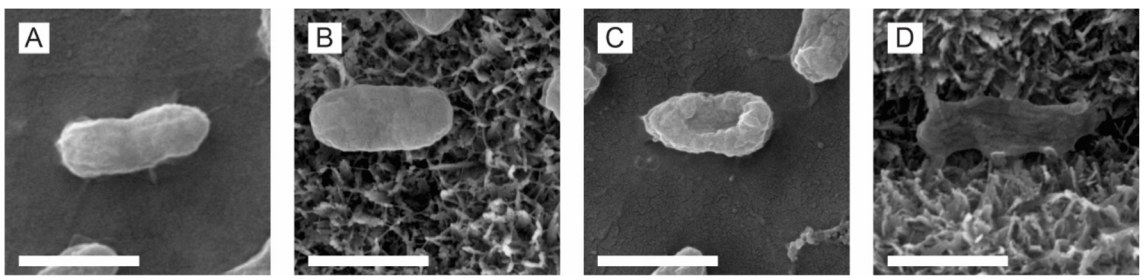

Fig. 3 Scanning electron microscope images of (A) live bacterial cells on a smooth titanium surface (control), (B) the live bacterial cells on the nanowire structured surface, (C) the dead bacterial cells on the smooth titanium surface (control), and (D) the dead *P. aeruginosa* bacterial cells on the nanowire structured surface. Bacterial cells were fixed with 2.5% glutaraldehyde and dehydrated with sequentially increasing concentrations of ethanol before dehydrating with HDMS. Samples were coated with a gold layer of 5 nm thickness. Scale bar: 1 µm.

substrates with smooth surfaces (A). The red colour indicates dead cells while the green colour in the images shows live cells. The control surface largely had live cells present, with very few noticeable dead cells (Fig. 5A). The 0.25 and 0.31 µm R_a surfaces showed a moderate number of dead cells present on them (Fig. 5B and C). However, the rest of the surfaces (Fig. 5D–H)

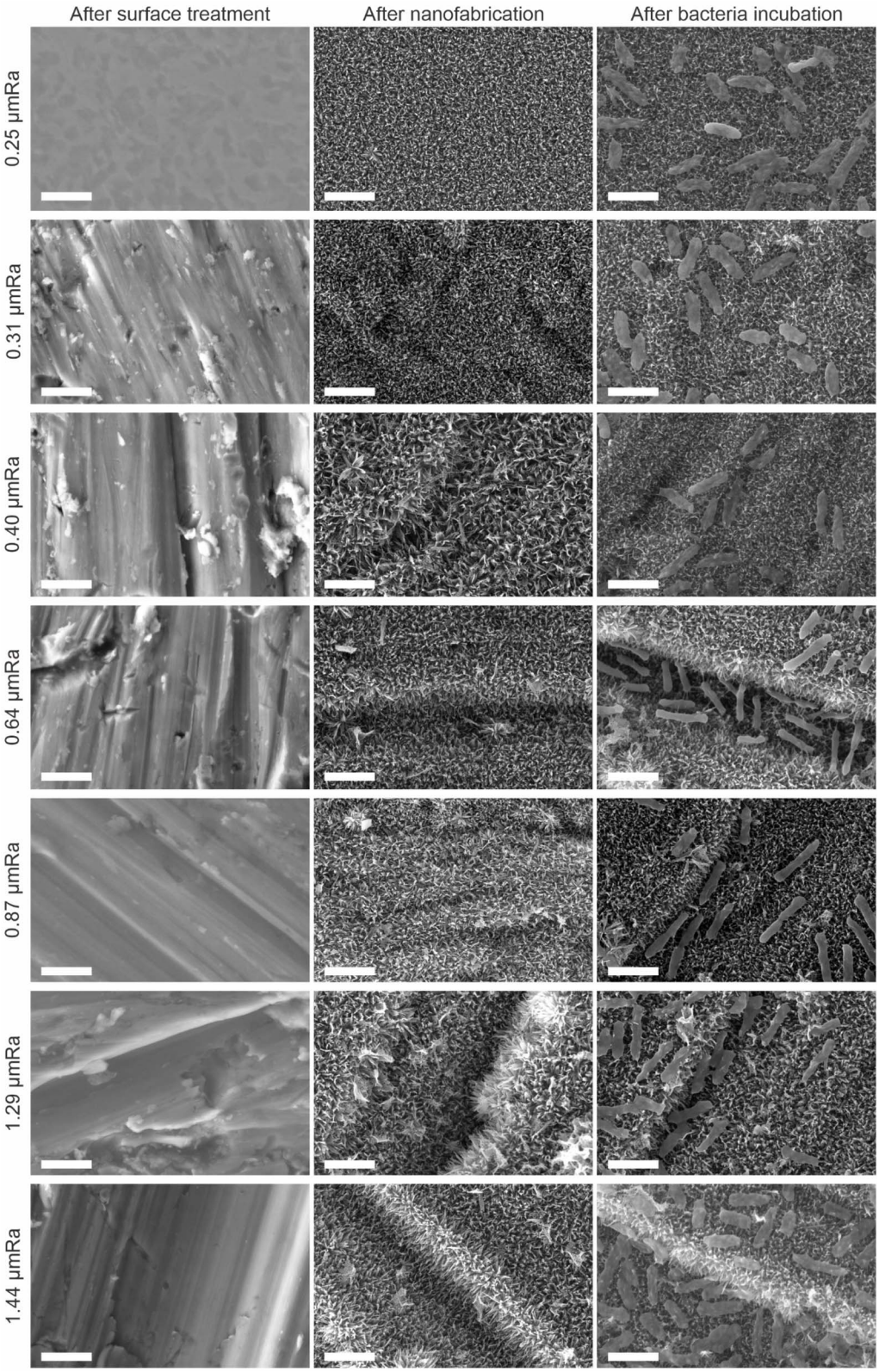

Fig. 4 Scanning electron microscope (SEM) images of the substrates, after surface finishing treatment (1st column), after nanowire fabrication using a hydrothermal treatment (2nd column), and after incubating with *P. aeruginosa* cells for 1 hour (3rd column). Scale bar: 2 μm.

mainly had dead cells present with few live cells on them. Moreover, the 0.87 μm R_a sample (Fig. 5F) was observed to have an extremely high surface coverage of cells compared to the other surfaces. The 0.87, 1.29, and 1.44 μm R_a surfaces were observed to have a linear pattern of dead cells that resembles their surface lay (Fig. 5F–H).

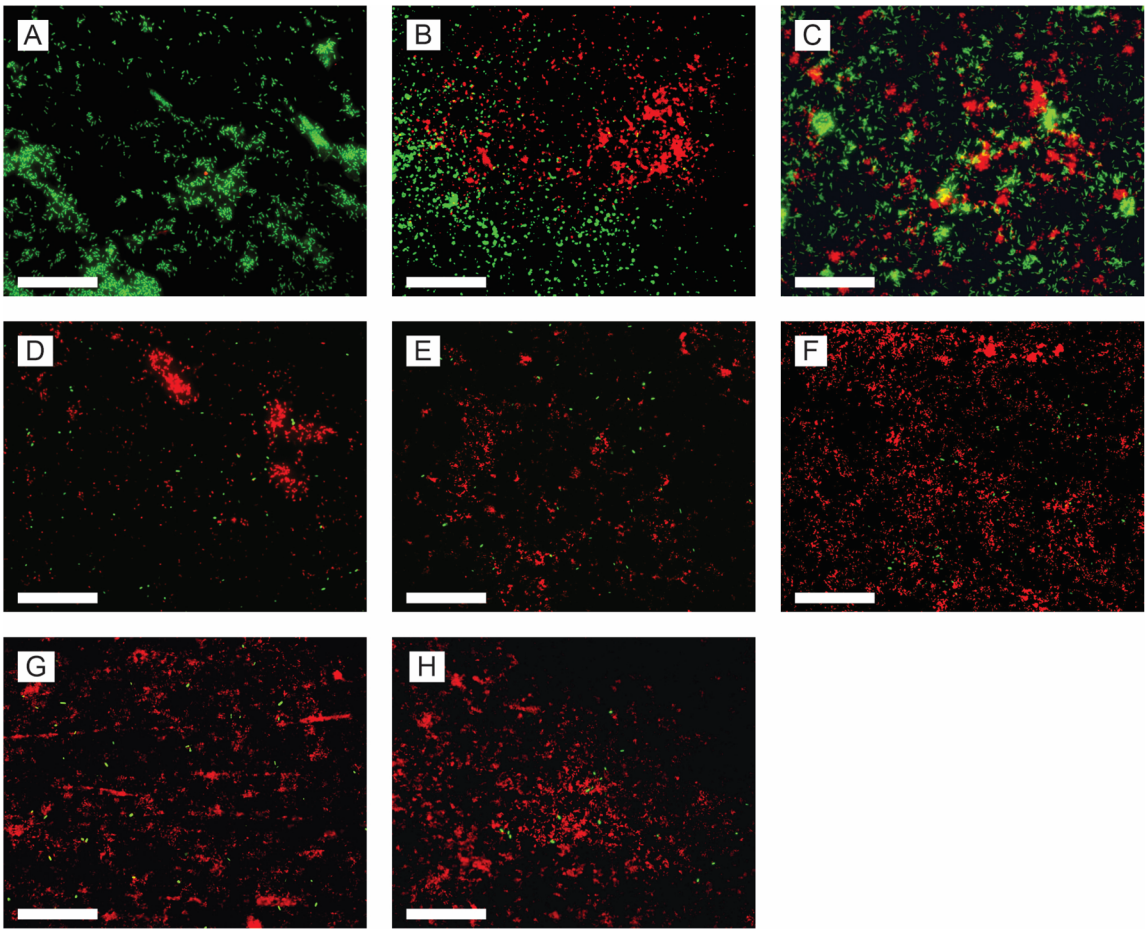

Fig. 5 Fluorescence images of the bacterial cells on (A) the control, (B) 0.25, (C) 0.31, (D) 0.40, (E) 0.64, (F) 0.87, (G) 1.29, and (H) 1.44 surfaces. Live cells are shown in green and dead cells are shown in red. The cells incubated on the surface were stained with a mixture of SYTO9 and PI then imaged using a fluorescence microscope with FITC and CY3 filters. Scale bar: 50 μm. The images show an area of 206.40 μm × 165.12 μm on the actual surface.

P. aeruginosa adhesion onto the surfaces

Fig. 6A shows the *P. aeruginosa* adhesion onto the 7 groups of nanostructured surfaces with varying macro surface roughness. Irrespective of the initial surface roughness, all hydrothermally treated titanium surfaces had a significantly lower bacterial adhesion ($p \leq 0.05$) compared to the untreated polished titanium surface (control) (data not shown). Notably, the number of cells adhered onto the 0.87 surface was significantly different from that of the 4 other groups namely, the 0.25, 0.31, 1.29, and 1.44 surfaces ($p < 0.05$). The adhesion in the 1.29 group was significantly different from the 0.40, and 0.64 groups in addition to the 0.87 group. Therefore, the 0.87 group promoted cell adhesion while the 1.29 and 1.44 surfaces had reduced bacterial adhesion onto the surface.

Bactericidal efficacy of the Ti nanostructured surfaces against *P. aeruginosa*

The bactericidal efficacy of the titanium nanostructured surfaces varied significantly when the macro surface roughness was varied, as shown in Fig. 6B. All hydrothermally treated surfaces, irrespective of the macro surface roughness, had significantly higher ($p \leq 0.02$) bactericidal efficacy than the untreated polished titanium surface (control) (data not shown).

The lowest bactericidal efficacy was observed on the 0.25 μm R_a surface (66.18% ± 21.61), and the highest was observed on the 0.87 μm R_a surface (91.60% ± 5.01). The bactericidal efficacy of the 0.25 μm R_a surface was significantly lower than all the other nanostructured surfaces, except for the 0.31 μm R_a surface. Despite the bactericidal efficacy increasing to 75% in the 0.31 group from 66% in the 0.25 group, the difference was not statistically significant ($p = 0.07$). Moreover, the 0.31 μm R_a surface showed significantly lower bactericidal efficacy than the 3 surfaces with highest surface roughness (0.87, 1.29, 1.44). A slight or no increase in bactericidal efficacy was observed from the 0.25 to 0.64 groups, but from the 0.64 to 0.87 groups, there was a large significant increase from 82% to 92%. Thereafter, there was no significant difference in bactericidal efficacy of the 0.87, 1.29, and 1.44 surfaces ($p > 0.99$). The bactericidal efficacy of the 0.87 group was significantly higher than all surfaces with lower surface roughness.

As Fig. 6C and D shows, the differences demonstrated in the bactericidal efficacies of the surfaces was mainly due to the differences in the number dead cells found on the surfaces.

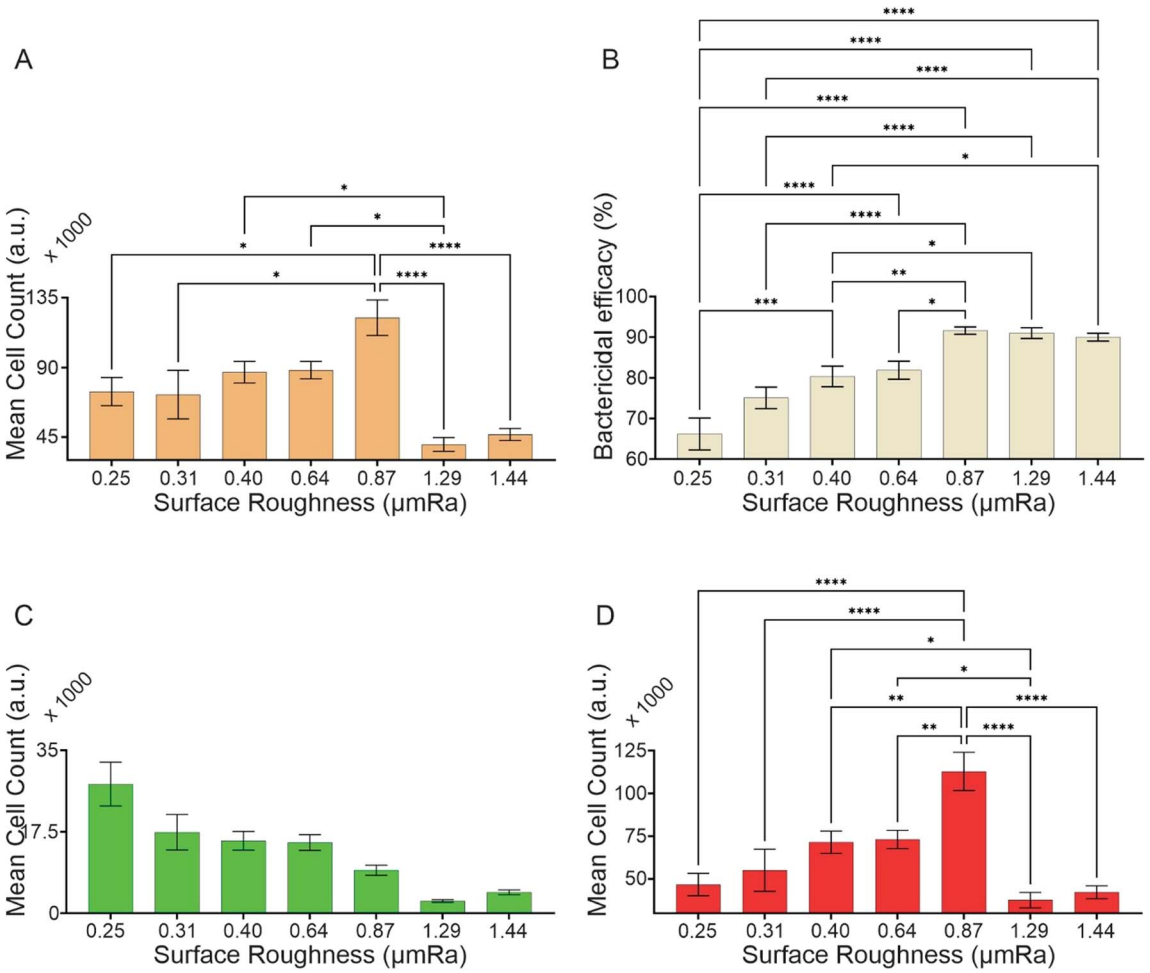

Fig. 6 (A) Total cell adhesion onto the treated (nanostructured) surfaces. (B) Bactericidal efficacy demonstrated by the surfaces. (C) Number of live bacterial cells and (D) number of dead cells remaining on the surfaces with varying initial macro surface roughness on titanium with hydrothermally fabricated nanowires. The 0.25 μm R_a titanium surface without nanowires was taken as the control and is not included in the graph. All live and dead cell counts were significantly different from their control counterparts. The cells incubated on the surface were stained with a mixture of SYTO9 and PI then imaged using a fluorescence microscope with FITC and CY3 filters. The cells were quantified by counting pixels of each image above a threshold level. The data are a mean of 30 images of 3 independent experiments ± standard error of the means. The bactericidal efficacy is taken as the number of dead cells ÷ the total number of cells (live + dead) on the surface. * shows statistical significance with ANOVA. Pairs with no significant($P > 0.05$) difference are not marked, *: $P \leq 0.05$, **: $P \leq 0.01$, ***: $P \leq 0.001$, and ****: $P \leq 0.0001$.

Fig. 6C shows that the live cell counts on the surfaces showed no significant variation with surface roughness ($p > 0.13$). Nevertheless, the nanowire structured surfaces showed significantly lower live cell counts than the smooth surface (data not shown). Fig. 6D shows the mean dead cell count on the 7 different nanowire structured surfaces tested. The dead cell counts on the nanowire structured surfaces were significantly higher than on the smooth surface (data not shown). The lowest number of dead cells, accounting for 37 626 ± 4413 units, was found on the 1.29 μm R_a surface, while the highest number of 112 862 ± 11 078 was found on the 0.87 μm R_a surface. Notably, the dead cell count on the 0.87 surface was significantly higher than on all the other surfaces, including the control surface ($p < 0.02$). Moreover, the dead cell count on the 1.29 surface was significantly lower than on the 0.64 and 0.40 surfaces. Other than those, none of the other compared groups had significant differences in dead cell counts. When the surface roughness was increased from 0.25 μm R_a, the dead cell count on the surface did not vary until the surface roughness was 0.87 μm R_a. It rose to 112 862 from 46 681 on the 0.25 surface and then dropped to 37 626 on the 1.29 surface. Therefore, the 0.87 μm R_a surface showed a notable spike in dead cell count when the surface roughness was varied from 0.25 to 1.44 μm R_a.

Correlation between macro surface roughness and cell adhesion and viability

XY data plots for bacterial adhesion, dead cell count, and the surface bactericidal efficacy are shown in Fig. 7A–C, respectively. The correlation analysis between the surface roughness and bacterial adhesion resulted in $r = -0.4696$ with $p = 0.29$, and hence the null hypothesis was accepted. This indicates a weak correlation between the two variables. Similarly, the correlation analysis between the dead cell count and surface roughness resulted in $r = -0.1953$ with $p = 0.68$, and therefore

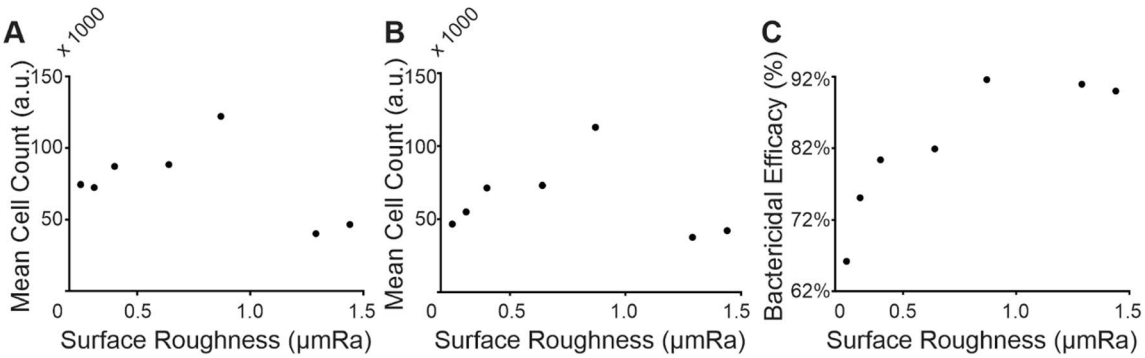

Fig. 7 *XY* correlation data for (A) bacterial adhesion, (B) dead cell count against the substrate surface roughness, and (C) bactericidal efficacy of the nanostructured surface.

the null hypothesis was accepted. A low Pearson coefficient means that the correlation between the dead cell count and surface roughness is weak. However, the correlation analysis between the surface roughness and bactericidal efficacy resulted in $r = 0.8535$ and $p = 0.01$ which indicates a strong correlation between the bactericidal efficacy and surface roughness.

Regression analysis for the bactericidal efficacy resulted in $R^2 = 0.6968$ for the linear regression and $R^2 = 0.8757$ for the non-linear quadratic regression. An *XY* scatter plot of the bactericidal efficacy shown in Fig. 7C also suggests that a quadratic function describes the relationship between surface roughness and bactericidal efficacy. The predicted regression model is given in eqn (4), where S is the surface roughness value in μm R_a.

$$\text{Bactericidal efficacy} = 55.19 + 65.63S - 29S^2 \quad (4)$$

Discussion

Increasing the roughness of the surface tends to increase its wettability.[62] The surfaces without nanostructures followed this theory but when the nanowires were fabricated using a hydrothermal treatment, even the finer surfaces became hydrophilic. The effect of the nanostructures on altering the hydrophobicity of a surface is well known.[63]

Nanowire structures of comparable size (tip diameter 25–50 nm) fabricated using a hydrothermal process on titanium surfaces with an initial surface roughness of ~0.25 μm R_a have shown bactericidal efficacy in the range of 50–70% against *P. aeruginosa* bacterial species when tested under static conditions.[32,34,46,58,64] The current study observed a bactericidal efficacy of 66% with the 0.25 μm R_a surface, which is comparable with the literature.

The 1.29 and 1.44 μm R_a groups showed a ~67% and 62% reduction in cell adhesion compared to the 0.87 μm R_a group ($p < 0.0001$) without compromising the bactericidal efficacy against the adherent bacteria. The SEM images show a deeper unidirectional surface lay on the two rougher surfaces compared to the 0.87 μm R_a surface. The SEM images of the surfaces with bacteria showed that the cells were less likely to attach onto the crest areas of the surface scratches. These crest areas are approximately less than 1 μm at their narrowest point and act like micron-sized knife blades. Therefore, the effective area at the crest is too small for bacteria to land on them and attach. The fluorescence images (Fig. 5) also complement this observation. The dead cells shown in red in those images can be seen to form lines, which could be the scratch marks on the surfaces.

The surface roughness of the titanium substrates used in this study obtained was by using abrasive sandpapers with a unidirectional reciprocating motion during the sanding

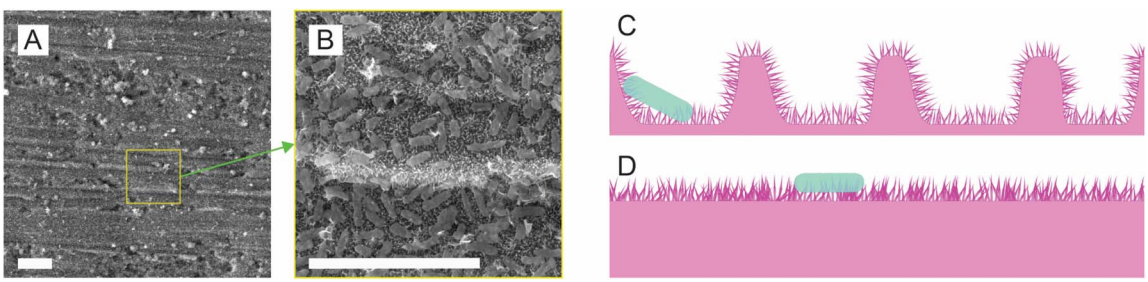

Fig. 8 (A) SEM image at 2k× magnification of the 1.44 μm R_a surface with *P. aeruginosa* bacteria on it. Scratch marks from the sanding surface can be seen on the surface (horizontal lines). (B) The same surface at 10k× magnification. The bacteria can be observed in the valley area of the scratch marks. Scale bar 10 μm. (C) Nanowires on the roughened substrate. The uneven topography of the roughened substrate leads to nanowires protruding from the surface in multiple directions and (D) the pictorial illustration (not to scale) of the nanowires on the smooth substrate.

process. This created characteristic unidirectional surface lay on the surface And the rougher surfaces had deeper scrapes on them. The SEM images showed a large concentration of bacterial cells in the valley areas, as shown in Fig. 8A and B. This macroscale topography has acted as traps for the bacterial cells. Moreover, in those valley areas, the bacterial cells can be pierced from multiple directions rather than from one direction. *P. aeruginosa* is a motile species of bacteria. The macro topography of the surface may have prevented the cells moving freely around, causing more cells to be present in between the peaks made by the surface scratches.

The surfaces with roughness values of 0.87, 1.29, and 1.44 μm R_a showed a notable increase in bactericidal effect compared to the surfaces with lower roughness. The roughness value represents the average depth of the micro-scale surface scratches (surface lay) on the surface. The *P. aeruginosa* cells in this study are approximately 0.5 × 1 μm in size and this is also reported in the literature as well.[65] The three surfaces with higher surface roughness have microscale trenches deeper than ~1 μm. This allows the cells to sink into the valley of the surface topography. Unlike on the flat topography, these micro trenches on the rough surfaces have nanowires present in multiple directions. This increased the possibility of the bacterial cell being pierced by a nanowire on the rough surface relative to those on the smooth surface. In addition, this rough topography may have hindered the movements of the motile *P. aeruginosa* cells causing them to be trapped in those valleys. Moreover, attempts by the cells to move in those rough terrains may also have contributed to increase bacterial death on the surface.

Surfaces with nanostructures, irrespective of their initial surface roughness, showed significant reduction in bacterial adhesion and viability, which has been proven previously.[50,56] Nanowire structures on titanium surfaces, similar to those used in this work, have previously been observed to be super hydrophilic.[66]

In the current study an attempt was made to obtain correlations between the surface roughness and cell adhesion or cell viability. The bactericidal efficacy of the surface was shown to have a correlation with the surface roughness through regression analysis. However, given the complexity of the variables involved, it would be very difficult to accurately model the relationship between the two entities. Nevertheless, the obtained correlation can still be used for further development of nanostructured surfaces for end user applications.

Conclusion

Macro surface roughness in the range of 0.87–1.44 μm R_a increases the bactericidal efficacy of nanowires fabricated on those surfaces. Classically, when nanowires are fabricated on titanium surfaces using a hydrothermal process, the initial surface roughness of the substrate is smoothed to a polished finish (surface roughness < 0.3 μm R_a). In terms of the bactericidal effect of the surface, this smoothing is not conducive to that effect. Since the smoothing of the initial substrate is not required for bactericidal efficacy, nanowires can be fabricated on a surface with any roughness without compromising the antibacterial properties. As the surface roughness correlates with the bactericidal efficacy, it can be used to manipulate the nanostructured surface for its bactericidal efficacy. Therefore, substrate surface roughness can be used as a parameter to optimize nanostructured surfaces, giving more flexibility for engineers to design application-oriented surfaces.

The macro surface roughness of the initial titanium substrate does not have a notable influence on the bacterial attachment onto the nanowire structures fabricated on them. However, when the surface contains large microscale surface features relative to the size of bacteria, the bacterial attachment is diminished. A multi-hierarchical surface topography is beneficial for increasing the bactericidal effect of nanowires. Microscale surface features that are close in size to the size of bacteria would increase the efficacy of the nanowire structured surface.

The current study is limited to the effect of a dual scale topography on *P. aeruginosa* cell adhesion and viability. Bacterial interactions with nanostructures are highly complex in nature and have been shown to be influenced by numerous factors including cell shape and size. Therefore, generalising the findings of this study may not be appropriate. Given this premise, it is worth investigating the effects of dual scale topography on different bacterial species with different morphologies, Gram stain types, *etc.* Furthermore, the dual scale topography can cause oxidative stress within bacterial cells as the cells could experience increased physical stress due to the topography. This phenomenon is worth exploring further.

Previous studies have shown that the bactericidal efficacy of nanostructures is increased under fluid flow conditions. Under a flow, bacterial cells are advected due to the fluid dynamic forces and collide with the sharp nanostructures causing more cell lysing. The dual scale topography on the surface may further aid this process resulting in more bacterial cell death on the surface. Further investigation of the effects of fluid flow is beneficial for developing antibacterial nanowires into industrial applications.

Regression analysis showed a correlation between bactericidal efficacy and (micro-scale) surface roughness. This analysis accounted for only the surface roughness with other contributory factors controlled. However, it is probable that interactions between those factors also affect the outcome.

Data availability

The data supporting this article have been included as part of the ESI. The following sets of data are included in the ESI† file submitted with the main article.

Author contributions

SWMAIS contributed to the conceptualisation, data curation, formal analysis, funding acquisition, investigation, methodology, validation, and writing of the original draft. PKDVY contributed to the conceptualisation, funding acquisition, project administration, resource, supervision, and review of the manuscript.

Conflicts of interest

There are no conflicts to declare.

Acknowledgements

The authors wish to acknowledge support and facilities from the Queensland University of Technology (QUT), Central Analytical Research Facility (CARF) of QUT, Centre for Biomedical Technologies (CBT). This project was funded by an ECR Seed Grant (2023) from the School of Mechanical, Medical, and Process Engineering, Queensland University of Technology, and the ARC Training Centre for M3D Innovation.

References

1 A. M. Valdes, J. Walter, E. Segal and T. D. Spector, Role of the gut microbiota in nutrition and health, *BMJ*, 2018, **361**, k2179.
2 Y.-J. Zhang, *et al.*, Impacts of Gut Bacteria on Human Health and Diseases, *Int. J. Mol. Sci.*, 2015, **16**, 7493–7519.
3 P. Hemarajata and J. Versalovic, Effects of probiotics on gut microbiota: mechanisms of intestinal immunomodulation and neuromodulation, *Therap. Adv. Gastroenterol*, 2013, **6**, 39–51.
4 K. S. Ikuta, *et al.*, Global mortality associated with 33 bacterial pathogens in 2019: a systematic analysis for the Global Burden of Disease Study 2019, *Lancet*, 2022, **400**, 2221–2248.
5 N. Kip and J. A. van Veen, The dual role of microbes in corrosion, *ISME J.*, 2015, **9**, 542–551.
6 B. J. Little, *et al.*, Microbially influenced corrosion—Any progress?, *Corros. Sci.*, 2020, **170**, 108641.
7 L. El-Bassi, I. Ziadi, S. Belgacem, L. Bousselmi and H. Akrout, Investigations on biofilm forming bacteria involved in biocorrosion of carbon steel immerged in real wastewaters, *Int. Biodeterior. Biodegradation*, 2020, **150**, 104960.
8 M. Salta, L. Capretto, D. Carugo, J. A. Wharton and K. R. Stokes, Life under flow: a novel microfluidic device for the assessment of anti-biofilm technologies, *Biomicrofluidics*, 2013, **7**, 064118.
9 L. F. Melo and T. R. Bott, Biofouling in water systems, *Exp. Therm. Fluid Sci.*, 1997, **14**, 375–381.
10 L. M. Brown, *et al.*, Community dynamics and phylogenetics of bacteria fouling Jet A and JP-8 aviation fuel, *Int. Biodeterior. Biodegradation*, 2010, **64**, 253–261.
11 S. Wang, *et al.*, Role of Lysinibacillus sphaericus on aviation kerosene degradation and corrosion of 7B04 aluminum alloy, *J. Mater. Res. Technol.*, 2022, **18**, 2641–2653.
12 J. S. Vrouwenvelder, D. A. Graf von der Schulenburg, J. C. Kruithof, M. L. Johns and M. C. M. van Loosdrecht, Biofouling of spiral-wound nanofiltration and reverse osmosis membranes: a feed spacer problem, *Water Res.*, 2009, **43**, 583–594.
13 J. D. Brooks and S. H. Flint, Biofilms in the food industry: problems and potential solutions, *Int. J. Food Sci. Technol.*, 2008, **43**, 2163–2176.
14 J. F. Cobo-Díaz, *et al.*, Microbial colonization and resistome dynamics in food processing environments of a newly opened pork cutting industry during 1.5 years of activity, *Microbiome*, 2021, **9**, 204.
15 B. Aslam, *et al.*, Antibiotic resistance: a rundown of a global crisis, *Infect. Drug Resist*, 2018, **11**, 1645–1658.
16 F. Prestinaci, P. Pezzotti and A. Pantosti, Antimicrobial resistance: a global multifaceted phenomenon, *Pathog. Glob. Health*, 2015, **109**, 309–318.
17 Centers for Disease Control and Prevention, *Antibiotic Resistance Threats*, 2013.
18 P. Shrestha, *et al.*, Enumerating the economic cost of antimicrobial resistance per antibiotic consumed to inform the evaluation of interventions affecting their use, *Antimicrob. Resist. Infect. Control*, 2018, **7**, 98.
19 X. Zhen, C. S. Lundborg, X. Sun, X. Hu and H. Dong, Economic burden of antibiotic resistance in ESKAPE organisms: a systematic review, *Antimicrob. Resist. Infect. Control*, 2019, **8**, 137.
20 World Bank, *Drug-Resistant Infections a Threat to Our Economic Future*, 2017.
21 S. W. M. A. I. Senevirathne, J. Hasan, A. Mathew, M. Woodruff and P. K. D. V. Yarlagadda, Bactericidal efficiency of micro- and nanostructured surfaces: a critical perspective, *RSC Adv.*, 2021, **11**, 1883–1900.
22 C. D. Bandara, *et al.*, Bactericidal Effects of Natural Nanotopography of Dragonfly Wing on Escherichia coli, *ACS Appl. Mater. Interfaces*, 2017, **9**, 6746–6760.
23 E. P. Ivanova, *et al.*, Natural bactericidal surfaces: mechanical rupture of pseudomonas aeruginosa cells by cicada wings, *Small*, 2012, **8**, 2489–2494.
24 J. Jenkins, *et al.*, Antibacterial effects of nanopillar surfaces are mediated by cell impedance, penetration and induction of oxidative stress, *Nat. Commun.*, 2020, **11**, 1626.
25 M. I. Ishak, *et al.*, Insights into complex nanopillar-bacteria interactions: roles of nanotopography and bacterial surface proteins, *J. Colloid Interface Sci.*, 2021, **604**, 91–103.
26 S. Zhao, *et al.*, Programmed Death of Injured Pseudomonas aeruginosa on Mechano-Bactericidal Surfaces, *Nano Lett.*, 2022, **22**, 1129–1137.
27 D. P. Linklater, V. A. Baulin, S. Juodkazis and E. P. Ivanova, Mechano-bactericidal mechanism of graphene nanomaterials, *Interface Focus*, 2018, **8**, 20170060.
28 S. P. S. N. B. S. Kumara, *et al.*, Progress in Nanostructured Mechano-Bactericidal Polymeric Surfaces for Biomedical Applications, *Nanomaterials*, 2023, **13**(20), 2799.
29 D. Linklater and E. P. Ivanova, Challenges to the design and testing of antimicrobial nanostructured surfaces, *Microbiol. Aust.*, 2023, **44**, 79–82.
30 E. P. Ivanova, *et al.*, Bactericidal activity of black silicon, *Nat. Commun.*, 2013, **4**, 2838.
31 G. Hazell, L. E. Fisher, W. A. Murray, A. H. Nobbs and B. Su, Bioinspired bactericidal surfaces with polymer nanocone arrays, *J. Colloid Interface Sci.*, 2018, **528**, 389–399.
32 C. M. Bhadra, *et al.*, Antibacterial titanium nano-patterned arrays inspired by dragonfly wings, *Sci. Rep.*, 2015, **5**, 1–12.

33 A. Jaggessar, S. W. M. A. I. Senevirathne, A. Velic and P. K. D. V. Yarlagadda, Antibacterial activity of 3D versus 2D TiO_2 nanostructured surfaces to investigate curvature and orientation effects, *Curr. Opin. Biomed. Eng.*, 2022, **23**, 100404.

34 S. W. M. A. I. Senevirathne, A. Mathew, Y. Toh and P. K. D. V. Yarlagadda, Bactericidal Efficacy of Nanostructured Surfaces Increases under Flow Conditions, *ACS Omega*, 2022, DOI: **10.1021/acsomega.2c05828**.

35 J. Macko, N. Podrojková, R. Oriňaková and A. Oriňak, New insights into hydrophobicity at nanostructured surfaces: experiments and computational models, *Nanomater. Nanotechnol.*, 2022, **12**, 1–21.

36 H. M. Shang, *et al.*, Nanostructured superhydrophobic surfaces, *J. Mater. Sci.*, 2005, **40**, 3587–3591.

37 M. Mu, *et al.*, Influence of Surface Roughness, Nanostructure, and Wetting on Bacterial Adhesion, *Langmuir*, 2023, **39**, 5426–5439.

38 J. Hasan, *et al.*, Multi-scale surface topography to minimize adherence and viability of nosocomial drug-resistant bacteria, *Mater. Des.*, 2018, **140**, 332–344.

39 A. Francone, *et al.*, Impact of surface topography on the bacterial attachment to micro- and nano-patterned polymer films, *Surf. Interfaces*, 2021, **27**, 101494.

40 K. Schwibbert, F. Menzel, N. Epperlein, J. Bonse and J. Krüger, Bacterial adhesion on femtosecond laser-modified polyethylene, *Materials*, 2019, **12**(19), 3107.

41 A. Velic, A. Jaggessar, T. Tesfamichael, Z. Li and P. K. D. V. Yarlagadda, Effects of nanopillar size and spacing on mechanical perturbation and bactericidal killing efficiency, *Nanomaterials*, 2021, **11**(10), 2472.

42 L. Wang, C. Hu and L. Shao, The antimicrobial activity of nanoparticles: present situation and prospects for the future, *Int. J. Nanomed.*, 2017, **12**, 1227–1249, DOI: **10.2147/IJN.S121956** Preprint at .

43 D. Acharya, *et al.*, Shape dependent physical mutilation and lethal effects of silver nanoparticles on bacteria, *Sci. Rep.*, 2018, **8**, 201.

44 S. W. M. A. I. Senevirathne. *Effect of Fluid Flow on Bacterial Attachment, Detachment, and Viability on Nanostructured Surfaces*, Queensland University of Technology, 2022, DOI: **10.5204/thesis.eprints.236965**.

45 A. Jaggessar and P. K. D. V. Yarlagadda, Modelling the growth of hydrothermally synthesised bactericidal nanostructures, as a function of processing conditions, *Mater. Sci. Eng. C*, 2020, **108**, 110434.

46 A. Jaggessar, *et al.*, Bacteria Death and Osteoblast Metabolic Activity Correlated to Hydrothermally Synthesised TiO2 Surface Properties, *Molecules*, 2019, **24**, 1201.

47 A. Jaggessar, S. W. M. A. I. Senevirathne, A. Velic and P. K. D. V. Yarlagadda, Antibacterial activity of 3D versus 2D TiO2 nanostructured surfaces to investigate curvature and orientation effects, *Curr. Opin. Biomed. Eng.*, 2022, **23**, 100404.

48 A. Jaggessar and P. K. D. V. Yarlagadda, Modelling the growth of hydrothermally synthesised bactericidal nanostructures, as a function of processing conditions, *Mater. Sci. Eng. C*, 2020, **108**, 110434.

49 A. Velic, J. Hasan, Z. Li and P. K. D. V. Yarlagadda, Mechanics of Bacterial Interaction and Death on Nanopatterned Surfaces, *Biophys. J.*, 2021, **120**, 217–231.

50 D. P. Linklater, S. Juodkazis, R. J. Crawford and E. P. Ivanova, Mechanical inactivation of Staphylococcus aureus and Pseudomonas aeruginosa by titanium substrata with hierarchical surface structures, *Materials*, 2019, **5**, 100197.

51 J. Hasan, S. Jain and K. Chatterjee, Nanoscale Topography on Black Titanium Imparts Multi-biofunctional Properties for Orthopedic Applications, *Sci. Rep.*, 2017, **7**, 1–13.

52 D. P. Linklater, H. K. D. Nguyen, C. M. Bhadra, S. Juodkazis and E. P. Ivanova, Corrigendum: Influence of nanoscale topology on the bactericidal efficiency of black silicon surfaces (2017 Nanotechnology 28 245301), *Nanotechnology*, 2017, **28**, 469501.

53 D. P. Linklater, S. Juodkazis, S. Rubanov and E. P. Ivanova, Comment on 'bactericidal Effects of Natural Nanotopography of Dragonfly Wing on Escherichia coli', *ACS Appl. Mater. Interfaces*, 2017, **9**, 29387–29393.

54 S. W. M. A. I. Senevirathne, Y.-C. Toh and P. K. D. V. Yarlagadda, Fluid Flow Induces Differential Detachment of Live and Dead Bacterial Cells from Nanostructured Surface, *ACS Omega*, 2022, **7**(27), 23201–23212.

55 S. W. M. A. I. Senevirathne, A. Mathew, Y. C. Toh and P. K. D. V. Yarlagadda, Preferential adhesion of bacterial cells onto top- and bottom-mounted nanostructured surfaces under flow conditions, *Nanoscale Adv.*, 2023, **5**, 6458–6472.

56 A. Jaggessar, *et al.*, Mechanical, bactericidal and osteogenic behaviours of hydrothermally synthesised TiO 2 nanowire arrays, *J. Mech. Behav. Biomed. Mater.*, 2018, **80**, 311–319.

57 X. Zhang, *et al.*, Comparing Two Functions for Optical Density and Cell Numbers in Bacterial Exponential Growth Phase, *J. Pure Appl. Microbiol.*, 2015, **9**(1), 299–305.

58 S. W. M. A. I. Senevirathne, Y.-C. Toh and P. K. D. V. Yarlagadda, Fluid Flow Induces Differential Detachment of Live and Dead Bacterial Cells from Nanostructured Surfaces, *ACS Omega*, 2022, **7**(27), 23201–23212.

59 S. W. M. A. I. Senevirathne, A. Mathew, Y. C. Toh and P. K. D. V. Yarlagadda, Preferential adhesion of bacterial cells onto top- and bottom-mounted nanostructured surfaces under flow conditions, *Nanoscale Adv.*, 2023, DOI: **10.1039/d3na00581j**.

60 M. I. Bogachev, *et al.*, Fast and simple tool for the quantification of biofilm-embedded cells sub-populations from fluorescent microscopic images, *PLoS One*, 2018, **13**(5), e0193267.

61 K. Y. Law, Definitions for hydrophilicity, hydrophobicity, and superhydrophobicity: getting the basics right, *J. Phys. Chem. Lett.*, 2014, **5**, 686–688, DOI: **10.1021/jz402762h** Preprint at .

62 J. Drelich and E. Chibowski, Superhydrophilic and superwetting surfaces: definition and mechanisms of control, *Langmuir*, 2010, **26**, 18621–18623.
63 P. A. Tran and T. J. Webster, Understanding the wetting properties of nanostructured selenium coatings: the role of nanostructured surface roughness and air-pocket formation, *Int. J. Nanomed.*, 2013, **8**, 2001–2009, DOI: **10.2147/IJN.S42970** Preprint at .
64 P. M. Tsimbouri *et al.*, *Osteogenic and Bactericidal Surfaces from Hydrothermal Titania Nanowires on Titanium Substrates*, Nature Publishing Group, 2016, pp. 1–12, DOI: **10.1038/srep36857**.
65 B. H. Iglewski, Pseudomonas, in *Medical Microbiology*, ed. S. Baron, 1996.
66 Q. Zhou, *et al.*, Rutile nanowire arrays: tunable surface densities, wettability and photochemistry, *J. Mater. Chem.*, 2011, **21**, 15806–15812.